# Correlation effects on Λ propagation in nuclear matter

N. J. Robertson* and W. H. Dickhoff†
*Department of Physics, Washington University, St. Louis, Missouri 63130, USA*
(Received 20 April 2004; published 4 October 2004)

The propagation of a Λ hyperon in nuclear matter is studied within the Green's function formalism. The probability density for adding a Λ hyperon with momentum $k$ to the correlated nuclear matter ground state is obtained from the complete energy dependence of the real and imaginary parts of the Λ self-energy. This self-energy incorporates the effects of short-range correlations induced by the hyperon-nucleon interaction and the strong coupling between Λ$N$ and Σ$N$ states which is known to be crucial for a correct determination of the Λ binding energy. The calculated spectral functions and quasi-particle parameters for the Λ are found to be qualitatively similar to corresponding results for correlated nucleons. In general, the Λ is less strongly correlated with the nuclear matter environment at $k_F = 1.36$ fm$^{-1}$ than a nucleon, in agreement with empirical information from finite nuclei.

DOI: 10.1103/PhysRevC.70.044301 PACS number(s): 21.80.+a, 21.65.+f

## I. INTRODUCTION

Hypernuclei, especially those with one Λ hyperon, have been studied for a long time [1,2]. When a Λ hyperon is placed in a nucleus or nuclear matter it will interact with the nucleons in its environment. As a result of these strong interactions, the Λ becomes correlated with nucleons in the medium. The study of the properties of the Λ hyperon in an environment of nucleons aims to answer a number of fundamental questions related to the properties of strange particles in the nuclear medium. Considerable attention has been given to the potential energy the Λ experiences in the nucleus and the corresponding single-particle (sp) energies. Experimental access to these sp energies is gleaned from associated production reactions of the $(\pi^+, K^+)$ type, strangeness exchange reactions involving $(K^-, \pi^-)$, and photoproduction (real or virtual) on a proton in the nucleus [3–5]. From this experimental work it becomes clear that the Λ hyperon is less strongly bound to nucleons than either a proton or a neutron. Such sp properties have been studied theoretically for finite nuclei by several groups [6–9]. The general conclusion from the experimental work is that the Λ hyperon experiences a potential well in the nucleus that has the familiar Woods-Saxon shape with a depth of about 30 MeV for a wide range of heavier nuclei. Additional information about the properties of Λ binding in the nucleus has been obtained from the study of the Λ self-energy for several nuclei [10,11].

Global sp properties of the Λ hyperon can be studied in nuclear matter. Results of such calculations have also been reported by several groups [12–18]. Important astrophysical information can be obtained from this type of work since it can be used to study the onset of hyperon formation in neutron stars [16,17,19] and the equation of state including hyperons [20–24]. The question of the stability of strange matter is of great interest and has been discussed for example in Refs. [25,26]. The relevance of strangeness for calculations of the properties of a neutron star has been discussed in Refs. [27,28].

The correlations of the Λ hyperon in nuclear matter have typically been studied at the level of its average binding or sp energy. The full propagator of the Λ including its complex self-energy has not been reported so far. The complex self-energy was studied in Ref. [10]. In view of the relevance of the properties of a strange particle in a nuclear system, it seems timely to elucidate the properties of a Λ hyperon when it is embedded in such a nuclear system. As in the case of nucleon-nucleon (*NN*) interactions, typical hyperon-nucleon (*YN*) interactions [29–34] incorporate substantial repulsion at short distance. The consequences of this strong interaction can be accounted for in the framework of the Green's function formalism by including the proper treatment of these short-range correlations (SRC) in the form of ladder-diagram summation for the hyperon-nucleon interaction in the medium ($G$ matrix). The effects on the dynamical single-particle properties of the Λ can then be explored by evaluating the complex self-energy of the Λ in nuclear matter. The solution of the Dyson equation for the Λ then again yields information on the net binding of the Λ in nuclear matter, but also determines the distribution of spectral strength for its addition to the nuclear-matter ground state as a result of SRC. Such calculations of the Λ spectral strength distribution will be reported for the first time in the present work.

Similar calculations of spectral functions have been performed for nucleons in nuclear matter (NM) for some time [35–39]. The addition of a strange test particle opens the door for quantitative comparisons with spectral functions obtained for nucleons and this avenue will be pursued in the present work. The weaker *YN* potential is expected to result in similar but less extreme modifications to the spectral distribution. However, the presence of the Λ hyperon also requires consideration of its heavier sibling, the isospin one Σ hyperon. The two hyperons have a small enough mass difference that a coupled channel problem must be solved. This is a change from the situation in pure nuclear matter, where

*Electronic address: njr@hbar.wustl.edu; http://www.artsci.wustl.edu/~njrobert
†Electronic address: wimd@wuphys.wustl.edu; http://www.physics.wustl.edu/~wimd

 

the explicit effect of the $\Delta$ isobar on nucleon propagation at low energy is normally ignored (see however Ref. [40]). As a result of this channel coupling, new structure arises in the $\Lambda$ spectral function which will be discussed in the present work.

A more detailed knowledge of the properties of a $\Lambda$ hyperon in nuclear matter may also be helpful in further elucidating the properties of the strangeness producing reactions on nuclei. Indeed, knowledge of the addition probability of a $\Lambda$ with a given momentum to the nuclear ground state is required for a more detailed microscopic description of the production of a $\Lambda$ in such reactions. The subsequent weak decay [41–44] of the $\Lambda$ after its production is another process where the information obtained in this work may be useful. Indeed, the nonmesonic weak decay of the $\Lambda$ requires another nucleon with which it will be strongly correlated. The consequences of the consistent inclusion of SRC on this weak decay will be reported elsewhere [45].

The paper starts with the introduction of the relevant formalism for the determination of the $\Lambda$ propagator in nuclear matter in Sec. II. After presenting some general formalism relevant for the description of a $\Lambda$ in nuclear matter, this section contains a detailed discussion in Sec. II A of the approximations made to the $\Lambda$ self-energy. The ingredients of the calculations are reviewed in Sec. II B. One important ingredient for these calculations is the *YN* interaction. In the present work, the soft-core version of Ref. [32] was chosen. The calculation of the effective *YN* interaction (*G* matrix) is presented in Sec. II C. Section III contains a presentation of the results with special emphasis on the underlying physics associated with the properties of a $\Lambda$ hyperon propagating in nuclear matter. Finally, conclusions are drawn in Sec. IV.

## II. FORMALISM

The results gathered in this section mainly pertain to the calculation of the $\Lambda$ propagator in the nuclear medium. Although no new results for nucleons are reported in this work, it is helpful to present some selected results related to the propagator of a nucleon in the nuclear medium. This facilitates the comparison between results obtained for the $\Lambda$ and the nucleon. We consider NM at a density corresponding to $k_F = 1.36$ fm$^{-1}$. The nucleon propagator, also called the Green's function, characterizes the excitation spectrum of a particle (or hole) created on top of the many-body ground state. The propagator formalism possesses features which make it especially useful for treating many-body systems consistently at various levels of approximation. Average single-particle observables as well as two-particle correlations can be extracted via the propagator formalism without the need to directly compute a many-body wave function. The appropriate choice for the sp basis in NM includes momentum, spin, isospin, and strangeness. We will employ the explicit notation $\Lambda$ or $\Sigma$ for the relevant hyperons in the present discussion and use the generic notation Y to denote either one.

Of particular relevance is the Lehmann representation of the sp propagator. For a nucleon in NM one obtains

$$g_N(\boldsymbol{k};\omega) = \int_{\varepsilon_F}^{\infty} d\omega' \frac{S_p(\boldsymbol{k};\omega')}{\omega - \omega' + i\eta} + \int_{-\infty}^{\varepsilon_F} d\omega' \frac{S_h(\boldsymbol{k};\omega')}{\omega - \omega' - i\eta}. \tag{1}$$

The Fermi energy, $\varepsilon_F$, has been introduced in Eq. (1) as the lowest energy above the ground state at which a particle may be added or the highest energy from which a particle can be removed. The spectral functions have the following form

$$S_p(\boldsymbol{k};\omega') \equiv |\langle \psi_n^{N+1}|a_{\boldsymbol{k}}^{\dagger}|\psi_0^N\rangle|^2 \frac{dn}{d\omega'}, \tag{2}$$

$$S_h(\boldsymbol{k};\omega') \equiv |\langle \psi_m^{N-1}|a_{\boldsymbol{k}}|\psi_0^N\rangle|^2 \frac{dm}{d\omega'} \tag{3}$$

for particles and holes, respectively. The factors $dn/d\omega'$ and $dm/d\omega'$ weight each term according to the density of states at an excitation energy of $\omega'$. We note that spin and isospin indices have been suppressed and in the following only the magnitude of the momentum vector will be used thereby taking into account the symmetries of NM. The particle spectral function, Eq. (2), denotes the probability density that a particle can be added to the NM ground state, $|\psi_0^N\rangle$, in a sp state $k$, at an excitation energy $\omega'$ of the $N+1$ particle system. Likewise, Eq. (3) describes the corresponding situation where a hole is added. As a probability density, the spectral function is real and positive. A particle (hole) occupation number may be defined for a state $k$ as the integrated strength above (below) the Fermi energy,

$$n_p(k) = \int_{\varepsilon_F}^{\infty} d\omega' S_p(k;\omega'), \tag{4}$$

$$n_h(k) = \int_{-\infty}^{\varepsilon_F} d\omega' S_h(k;\omega'). \tag{5}$$

The total spectral strength, $S = S_p + S_h$ is normalized in such a way that

$$\int_{-\infty}^{\infty} d\omega' S(k;\omega') = n_p(k) + n_h(k) = 1. \tag{6}$$

From Eq. (1) one obtains that the spectral functions are related to the imaginary part of the propagator by

$$S_p(k;\omega) = -\frac{1}{\pi}\mathrm{Im}\, g(k;\omega), \quad \omega > \varepsilon_F \tag{7}$$

for the particle addition probability density and

$$S_h(k;\omega) = \frac{1}{\pi}\mathrm{Im}\, g(k;\omega), \quad \omega < \varepsilon_F \tag{8}$$

for the removal probability.

In the case of the $\Lambda$ propagator some qualitative changes occur in comparison with the case of the nucleon propagator. The result corresponding to Eq. (1) now becomes

$$g_\Lambda(k;\omega) = \int_{\varepsilon_T^\Lambda}^{\infty} d\omega' \frac{S_\Lambda(k;\omega')}{\omega - \omega' + i\eta}. \quad (9)$$

Since no Fermi surface for Λ hyperons is considered in this work, it is not possible to remove a Λ from the NM ground state. As a result, the propagator only contains the probability amplitude for adding a Λ particle with momentum $k$ at an energy $\omega'$. This particle spectral function for the Λ is given by

$$S_\Lambda(k;\omega') \equiv |\langle \psi_{n,\Lambda}^{N+1} | a_{k,\Lambda}^\dagger | \psi_0^N \rangle|^2 \frac{dn}{d\omega'}. \quad (10)$$

The energy threshold at which it becomes possible to add a Λ to the NM ground state is denoted by $\varepsilon_T^\Lambda$. One expects this energy to be accessible only for a Λ at rest ($k=0$). If the Λ were added to a free Fermi gas NM ground state and would not be correlated otherwise, this threshold energy would simple be the kinetic energy of a Λ with zero momentum and would therefore correspond to zero energy. Based on previous work by other groups [14,16] one expects the actual value of the threshold energy at normal NM density to be around −30 MeV indicating the substantial attraction a Λ experiences in NM. Since the Λ can only propagate as a particle, the spectral strength above the threshold energy must integrate to 1. This condition on the Λ spectral function is given by

$$\int_{\varepsilon_T^\Lambda}^{\infty} d\omega' S_\Lambda(k;\omega') = n_{p,\Lambda}(k) = 1. \quad (11)$$

This result is quite different from the corresponding nuclear one given by Eq. (6) where a split between the occupied and unoccupied strength occurs. As in the case of nucleons one can obtain the spectral function from the imaginary part of the propagator,

$$S_\Lambda(k;\omega) = -\frac{1}{\pi} \mathrm{Im}\, g_\Lambda(k;\omega), \quad \omega > \varepsilon_T^\Lambda. \quad (12)$$

It is practical to list the corresponding results for noninteracting propagators. The noninteracting propagator for the nucleon is given by

$$g_N^{(0)}(k;\omega) = \frac{\theta(k-k_F)}{\omega - \varepsilon_N(k) + i\eta} + \frac{\theta(k_F-k)}{\omega - \varepsilon_N(k) - i\eta}. \quad (13)$$

This result demonstrates that $g_N^{(0)}(k;\omega)$ contains only a simple pole at an excitation energy corresponding to the energy of the sp state. The spectral functions [Eqs. (7) and (8)] for the noninteracting case are

$$S_p^{(0)}(k;\omega) = \theta(k-k_F)\delta(\omega - \varepsilon_N(k)), \quad (14)$$

$$S_h^{(0)}(k;\omega) = \theta(k_F-k)\delta(\omega - \varepsilon_N(k)). \quad (15)$$

Equations (14) and (15) indicate that a nucleon may be added to, for $k>k_F$, or removed from the medium, for $k<k_F$, in a sp state $k$, with unit strength, at an energy corresponding to $\varepsilon(k)$, and not at any other energy. The propagator for a noninteracting Λ hyperon is given by

$$g_\Lambda^{(0)}(k;\omega) = \frac{1}{\omega - \varepsilon_\Lambda(k) + i\eta}. \quad (16)$$

The result for the corresponding spectral function then reads

$$S_\Lambda^{(0)}(k;\omega) = \delta(\omega - \varepsilon_\Lambda(k)). \quad (17)$$

The actual choice of the single-particle spectrum contained in $\varepsilon_\Lambda(k)$ or [$\varepsilon_N(k)$ for the nucleon] usually only contains the kinetic energy contribution [$t_\Lambda(k)=k^2/2m_\Lambda$ in the case of the Λ]. The addition of strong interactions amongst the particles, which induce correlations, changes this picture. The dressed propagator will have a more complex analytic structure as a function of energy, which gives rise to a correspondingly rich structure in the spectral function as indicated in Eqs. (1) and (9). The relation between the dressed and noninteracting propagators is provided by the Dyson equation which is discussed in standard textbooks [46,47]. For both a nucleon and a Λ in the medium the Dyson equation takes the form

$$g(k;\omega) = g^{(0)}(k;\omega) + g^{(0)}(k;\omega)\Sigma(k;\omega)g(k;\omega), \quad (18)$$

where terms in the propagator expansion have been arranged in such a way that the self-energy, Σ, is irreducible. The Dyson equation may be solved algebraically to yield

$$g(k;\omega) = \frac{1}{\omega - \varepsilon(k) - \Sigma(k;\omega)}. \quad (19)$$

This formal solution should be compared with Eqs. (13) and (16) for the noninteracting propagator of a nucleon and a Λ, respectively. The essential difference lies in the presence of the self-energy which acts as an effective potential for the nucleon or the Λ. A truncation of the self-energy expansion at some finite order in the interaction is not a viable option for the strong interactions commonly used in nuclear physics. The individual terms may even be divergent if interactions with hard-cores are used. Instead, approximations are required which involve summing an infinite number of terms taken from those classes of diagrams deemed most important for a given calculation. The relevant set of terms needed to obtain sensible results at the two-body level has since long been identified as the set of diagrams involving repeated interactions between the particles to all orders as in the $T$-matrix in free space. The inclusion of these terms in the self-energy is expected to give the most important correction to the Hartree-Fock contribution to the self-energy since it correctly treats the effect of SRC on the sp properties. The essential ingredients to be considered for this approximation are gathered in the next subsection.

### A. Approximation to the Λ self-energy

The Hartree-Fock (HF) contribution to the self-energy of a Λ in nuclear matter is given by

$$\Sigma_\Lambda^{HF}(k) = \sum_{k'} \int_{\varepsilon_F}^{\infty} \frac{d\omega'}{2\pi i} e^{i\omega'\eta} \langle kk'|V|kk'\rangle g_N(k';\omega'),$$
$$= \sum_{k'} \int_{\varepsilon_F}^{\infty} d\omega' \langle kk'|V|kk'\rangle S_h(k';\omega')$$
$$= \sum_{k'} \langle kk'|V|kk'\rangle n_h(k'), \tag{20}$$

which may be simply interpreted as an average over the interactions between the $\Lambda$ and the nucleons in the ground state characterized by the momentum distribution $n_h$. Here and in the following the first member of a two-body state refers to a hyperon and the second to a nucleon. To simplify notation only the magnitude of the momentum quantum number is indicated. In addition to the direction of the momentum this quantum number therefore also implicitly refers to spin and isospin in the case of nucleons. In the case of a hyperon also the specific hyperon under consideration is implicated ($\Lambda$ or $\Sigma$ hyperon). More explicit results are formulated in the next subsection where details of the actual calculation are discussed. The convergence factor in the first equality in Eq. (20) ensures that only the contribution of particles that are present in the medium are considered. A requirement of the bare *YN* interaction is that it provides a realistic description of free-particle scattering at low energies (typically up to pion production threshold). Such an interaction will be real, strongly repulsive at short range and moderately attractive at longer range. Matrix elements, taken in the uncorrelated *YN* basis, are on average repulsive. As a result, the HF self-energy will be real and positive, acting as a repulsive mean-field potential which shifts the $\Lambda$ spectrum to

$$\varepsilon_\Lambda^{HF}(k) = t_\Lambda(k) + \Sigma_\Lambda^{HF}(k). \tag{21}$$

This is not a realistic approximation in two respects. Despite the strong repulsive core in realistic nuclear and hypernuclear potentials, there is a net attraction, as evidenced by the existence of bound nuclei and hypernuclei. The HF approximation yields a real self-energy, which implies an Independent Particle Model (IPM). Particles occupy sp states with infinite lifetimes. Despite its limitations, the HF approximation provides an intuitive method for generating a mean-field from a two-body interaction and is the simplest non-trivial approximation which allows a self-consistent treatment of the many-body problem.

The deficiencies alluded to above can be overcome by replacing the bare two-body interaction, *V*, with an effective interaction which is both complex and has a real part which is on average attractive. An effective interaction which possesses the necessary traits to include SRC may be derived from the bare interaction by summing all the ladder diagrams depicted graphically in Fig. 1(a). In the limit of zero density (the interaction of two free particles) this effective interaction is just the *T* matrix of scattering theory. When a medium is present, restrictions on particle propagation exist related to the presence of the (possibly correlated) Fermi sea. If the intermediate particles correspond to mean-field particles and are not dressed, then the effective, in-medium interaction is called the Brueckner *G*-matrix. If the intermediate propagators are dressed, this generalized version of the *G* matrix will be called the $\Gamma$ matrix [48]. The series of ladder diagrams may be resummed in two ways as illustrated in Fig. 1. Figure 1(a) depicts the integral equation for the $\Gamma$ matrix in terms of *V* and the uncorrelated but possibly dressed two-particle propagator indicated by the parallel double lines. These particles in the intermediate state may be separately dressed by interactions with the medium, but are not correlated with each other. After suitable approximations are made this form of the $\Gamma$ matrix equation has been used in the calculation of the $\Lambda$ self-energy and will be discussed in more detail in the next subsection. An alternative, but entirely equivalent, resummation leads to Fig. 1(b). Here the $\Gamma$ matrix is expressed in terms of *V* and the correlated $\Lambda N$ two-particle propagator. This version of the ladder equation is useful for elucidating an important analytic property of the $\Gamma$ matrix. The diagrammatic expression of Fig. 1(b) is represented by

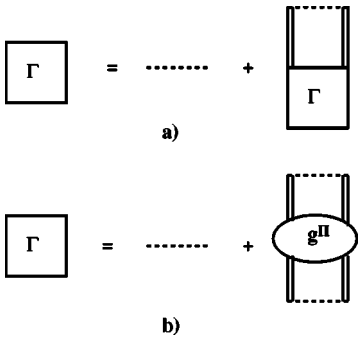


FIG. 1. Ladder equation for the effective interaction, *G*, in terms of a) uncorrelated (but in principle dressed) two-particle propagator and b) correlated two-particle propagator.

$$\langle kk'|\Gamma(\Omega)|kk'\rangle = \langle kk'|V|kk'\rangle + \sum_{k_1k_2k_1'k_2'} \langle kk'|V|k_1k_2\rangle \times g_{YN}^{II}(k_1k_2,k_1'k_2';\Omega)\langle k_1'k_2'|V|kk'\rangle. \tag{22}$$

The energy dependence is entirely contained in the correlated *YN* propagator. It should be observed that this propagator contains both diagonal ($\Lambda N$ and $\Sigma N$) as well as nondiagonal contributions in the hyperon quantum numbers ($\Lambda N$-$\Sigma N$ or $\Sigma N$-$\Lambda N$). In direct analogy with the sp propagator one can obtain a Lehmann representation for this propagator in the following form

$$g_{YN}^{II}(k_1k_2,k_1'k_2';\Omega) = \int_{\Omega_{min}}^{\infty} d\Omega' \frac{S_{YN}(k_1k_2,k_1'k_2';\Omega')}{\Omega - \Omega' + i\eta}. \tag{23}$$

The two-particle spectral density function,

$$S_{YN}(k_1k_2,k_1'k_2';\Omega') \equiv \langle \psi_0^N|a_{k_1}a_{k_2}|\psi_n^{N+2}\rangle\langle\psi_n^{N+2}|a_{k_1'}^\dagger a_{k_2'}^\dagger|\psi_0^N\rangle \frac{dn}{d\Omega'} \tag{24}$$

has been introduced, much like the sp spectral function of Eq. (2). The threshold energy for *YN* propagation is the lowest energy for which a $\Lambda$ and a nucleon can be added to the ground state of nuclear matter and is therefore given by

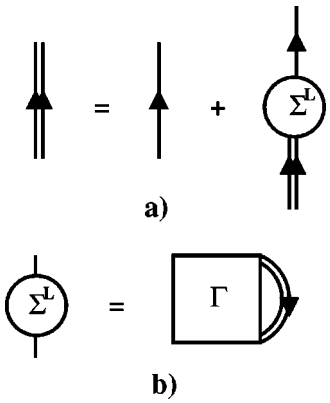


FIG. 2. Diagrammatic representation of Dyson's equation in the ladder approximation. Part (a) shows the Dyson equation. The self-energy has been provided with superscript ***L*** to emphasize that this represents the approximation shown in part b) which includes the effective interaction shown in Fig. 1.

$$\Omega_{min} = \varepsilon_F + \varepsilon_T^{\Lambda}. \tag{25}$$

The analytic structure of the correlated *YN* propagator mirrors that of the sp propagator in its simplicity. In particular, one can obtain the following dispersion relation

$$g_{YN}^{II}(k_1k_2,k_1'k_2';\Omega) = -\frac{1}{\pi}\int_{\Omega_{min}}^{\infty} d\Omega' \frac{\mathrm{Im}\, g_{YN}^{\mathrm{II}}(k_1k_2,k_1'k_2';\Omega')}{\Omega - \Omega' + i\eta}. \tag{26}$$

Insertion of this expression for $g_{YN}^{II}$ into Eq. (22) for the Γ matrix yields

$$\langle kk'|\Gamma(\Omega)|kk'\rangle = \langle kk'|V|kk'\rangle - \frac{1}{\pi}\int_{\Omega_{min}}^{\infty} d\Omega' \frac{\mathrm{Im}\,\langle kk'|\Gamma(\Omega')|kk'\rangle}{\Omega - \Omega' + i\eta} \tag{27}$$

as a dispersion relation for the Γ matrix. This result illustrates that it is possible to obtain the real part of the Γ matrix as a dispersion integral over the imaginary part which is required for all energies above $\Omega_{min}$. Since both the real and imaginary part of Γ are calculated at a given energy, one may use Eq. (27) as a consistency check on the numerical calculation of the Γ-matrix.

The Λ self-energy in the ladder approximation (LA) may be compactly represented as in Fig. 2. In part (a) of this figure the Dyson equation is shown. Part (b) illustrates the self-energy when the effective interaction is represented by the ladder-summed effective interaction shown in Fig. 1(a). This result may be compared to the HF approximation. In that case Γ is replaced by the bare interaction indicated by the dashed line in Fig. 1. The self-energy may still be thought of as an effective potential for the Λ as generated by its average interaction with the nucleons. The difference is that the bare interaction is now replaced by the Γ matrix effective interaction. The Γ matrix is complex and energy dependent, satisfying the list of desirable qualities mentioned previously for an effective two-particle interaction. In addition, it has the distinction of being derived directly in terms of the bare interaction.

The simplicity of the diagram [Fig. 2(b)] expressing the self-energy in terms of the Γ matrix reflects a simple mathematical relationship between the two functions:

$$\Sigma_\Lambda(k;\omega) = \sum_{k'} \int \frac{d\omega'}{2\pi i} e^{i\omega'\eta} \langle kk'|\Gamma(\omega+\omega')|kk'\rangle g_N(k';\omega') = \sum_{k'} \int_{-\infty}^{\varepsilon_F} d\omega' \langle kk'|\Gamma(\omega+\omega')|kk'\rangle S_h(k';\omega'). \tag{28}$$

The spectral representation of the nucleon hole propagator [Eq. (1)] was used to obtain the final expression of Eq. (28). Similar to the HF case [Eq. (20)] which is contained in Eq. (28), the self-energy in the LA is just a convolution of the effective interaction with the spectral density of occupied nucleon states, although in the present case it also requires knowledge of the energy dependence of the nucleon hole strength. Just as the Γ matrix satisfies a dispersion relation, so too does the self-energy. Inserting Eq. (27) into Eq. (28) yields

$$\Sigma_\Lambda(k;\omega) = \sum_{k'} \langle kk'|V|kk'\rangle n_h(k') + \int_{\Omega_{min}}^{\infty} d\omega' \frac{\mathrm{Im}\,\Sigma_\Lambda(k;\omega')}{\omega - \omega' + i\eta} = \Sigma_\Lambda^{HF}(k) + \Sigma_\Lambda^{\Delta}(k;\omega). \tag{29}$$

### B. Ingredients of the calculation

Having chosen the LA as a physically suitable approximation to Dyson's equation (Fig. 2), the framework is set for the calculation of the Λ propagator. Now it is necessary to consider the ingredients that are required to explicitly implement this scheme in a tractable manner. A major ingredient is the two-body interaction which describes the scattering of hyperons and nucleons. We have chosen a Nijmegen Soft Core (NSC89) meson exchange potential [32]. This potential is the Fourier transformable, soft-core descendant of the hard-core Nijmegen D and F models [29–31]. In the microscopic spirit of this work, it is based on the exchange of mesons. Though fit to available *YN* scattering data, the scarcity of such data demands a heavy reliance on SU(3) symmetries to relate poorly determined *YN* coupling constants to their better known *NN* relatives. As with all potentials of this type, the NSC89 is fit to low-energy data and its core structure is not well determined. Results which depend on the short-range behavior of the potential will reflect this deficiency but are consequently of interest as well. The more recent versions of this potential as presented in Ref. [34] have been shown to overbind single hypernuclei [24] and were not considered for the present calculation at this time.

The *NN* interaction appears implicitly in the nucleon propagators with which the Λ interacts. Results for these nucleon propagators are based on calculations [39] involving the Reid Soft Core (RSC) potential [49]. The nucleon hole and particle propagators appear in the self-energy equation [Fig. 2(b)] and the Γ-matrix equation [Fig. 1(a)] as external

parameters. This illustrates the obvious statement that one does not have to recalculate nucleon properties after introducing a single $\Lambda$ hyperon in the medium. In principle, the dressed nucleon propagator should be determined from a coupled system of equations similiar to those depicted in Figs. 1 and 2. In this work, we will approximate the dressed propagator by only including the self-consistent sp spectrum as obtained in Ref. [39]. As a result the nucleon propagator retains the form of the noninteracting propagator [see Eq. (13)] but has a sp spectrum that is determined by the real part of the self-energy of the nucleon. The $\Sigma$ hyperon has been introduced as part of a possible *YN* intermediate state in the $\Gamma$ matrix equation [Fig. 1(a)]. Its inclusion is necessitated by the relatively small mass difference of about 77 MeV between the $\Lambda$ and $\Sigma$. This results in a significant coupling between $\Lambda N$ and $\Sigma N$ intermediate states which cannot be ignored. It is probably correct to conclude that the experimental and theoretical analysis of $\Sigma$ bound states suggest little if any binding for this hyperon in nuclei [50]. Compared with sp potential well depths of approximately 30 MeV for the $\Lambda$ and 75 MeV for the nucleon in NM, the $\Sigma$ interacts relatively weakly with the nuclear medium even though about 15 MeV binding is obtained in NM in our calculation confirming the result obtained in Ref. [17]. It is therefore a reasonable approximation to treat the $\Sigma$ as a particle which only has a modified sp energy in the medium as is done in this work. The resulting propagator is then of the form of Eq. (16). The modification of the sp energy is obtained in the same way as described for the $\Lambda$ below.

At this point it is useful to note that although the $\Lambda$ propagator has a formal solution in terms of the self-energy, the self-energy depends internally on the dressed propagator. This means that Figs. 1 and 2 depict a coupled system of equations for the dressed $\Lambda$ propagator. The natural starting point is to make the zeroth order approximation

$$g_\Lambda(k;\omega) \to g_\Lambda^{(0)}(k;\omega). \tag{30}$$

Given this choice of initial $\Lambda$ propagator, the $\Gamma$-matrix, self-energy, and next generation propagator may be calculated in turn. Ideally, one would now like to use this new propagator, $g_\Lambda^{(1)}(k;\omega)$, as input to the $\Gamma$-matrix equation and iterate until a self-consistent solution is obtained. Examination of Eq. (19) reveals that the energy dependence of the dressed propagator is much more complicated than that of the free propagator, Eq. (16). In fact, this is also true for $g_\Lambda^{(1)}(k;\omega)$, which has an analytic structure similar to that of the fully self-consistent propagator, even after only one interation. A simplified iteration scheme is therefore used instead.

Breaking up the self-energy into its real and imaginary parts, Eq. (19) for the dressed propagator can be rewritten as:

$$g_\Lambda(k;\omega) = \frac{1}{[\omega - t_\Lambda(k) - \mathrm{Re}\,\Sigma_\Lambda(k;\omega)] - i[\mathrm{Im}\,\Sigma_\Lambda(k;\omega)]}. \tag{31}$$

Comparing this to the form of the free propagator, Eq. (16), it can be seen that the real part of the self-energy plays the role of an energy-dependent potential. This observation motivates the definition of a new energy spectrum:

$$\varepsilon_\Lambda^{(1)}(k) = t_\Lambda(k) + \mathrm{Re}\,\Sigma_\Lambda(k;\varepsilon_\Lambda^{(1)}(k)). \tag{32}$$

This new spectrum, which will later be identified as the quasi-particle (qp) energy spectrum, is inserted in place of the kinetic energy spectrum in Eq. (16), to define a new propagator

$$g_\Lambda^{(1)}(k;\omega) \to \tilde{g}_{(1)}^\Lambda(k;\omega) \equiv \frac{1}{\omega - \varepsilon_\Lambda^{(1)}(k) + i\eta}. \tag{33}$$

In this way, the same simple analytic structure is always used for the $\Lambda$ propagator in the $\Gamma$ matrix equation, and only the spectrum changes from iteration to iteration. The iteration procedure is continued until a self-consistent Lambda spectrum is obtained:

$$\varepsilon_\Lambda^{(n+1)}(k) = \varepsilon_\Lambda^{(n)}(k). \tag{34}$$

As will be discussed later, it is important to calculate such a consistent spectrum in order to ensure that the final spectral function is a continuous function of energy. It should be noted here that this approximation in obtaining the $\Lambda N$ effective interaction is equivalent to the usual *G* matrix procedure. For this reason, we will adapt this notation for this interaction from now on.

After obtaining self-consistency according to Eq. (34), the spectral function is calculated from the imaginary part of the dressed propagator, Eq. (31) using the expression of Eq. (12).

$$S_\Lambda(k;\omega) = \frac{1}{\pi}\frac{|\mathrm{Im}\,\Sigma_\Lambda^{(s)}(k;\omega)|}{[\omega - t_\Lambda(k) - \mathrm{Re}\,\Sigma_\Lambda^{(s)}(k;\omega)]^2 - i[\mathrm{Im}\,\Sigma_\Lambda^{(s)}(k;\omega)]^2}. \tag{35}$$

The self-energy bears an "*s*" superscript to denote the fact that it is calculated using a self-consistent $\Lambda$ spectrum. It should be emphasized that the spectral function of Eq. (35) is *not* truly self-consistent due to the simplifying approximation of Eq. (33). A qp energy can now be defined as in Eq. (32),

$$\varepsilon_\Lambda^{qp}(k) = t_\Lambda(k) + \mathrm{Re}\,\Sigma_\Lambda^{(s)}(k;\varepsilon_\Lambda^{qp}(k)). \tag{36}$$

If the self-energy is only weakly energy dependent in the neighborhood of the qp energy, then it is evident from Eq. (35) that the spectral function will have a peak near $\varepsilon_\Lambda^{qp}(k)$. Expanding the self-energy about $\varepsilon_\Lambda^{qp}(k)$ as

$$\mathrm{Re}\,\Sigma_\Lambda^{qp}(k;\omega) \equiv \mathrm{Re}\,\Sigma_\Lambda^{(s)}(k;\varepsilon_\Lambda^{qp}(k)) + \frac{\partial\,\mathrm{Re}\,\Sigma_\Lambda^{(s)}(k;\varepsilon_\Lambda^{qp}(k))}{\partial\,\omega}(\omega - \varepsilon_\Lambda^{qp}(k)), \tag{37}$$

$$\mathrm{Im}\,\Sigma_\Lambda^{qp}(k) \equiv \mathrm{Im}\,\Sigma_\Lambda^{(s)}(k;\varepsilon_\Lambda^{qp}(k)), \tag{38}$$

yields the qp approximation to the spectral function. We define the following two functions

$$z(k) \equiv 1 - \left[\frac{\partial\,\mathrm{Re}\,\Sigma_\Lambda^{(s)}(k;\omega)}{\partial\,\omega}\right]^{-1}, \tag{39}$$

$$\gamma(k) \equiv z(k)|\mathrm{Im}\,\Sigma_\Lambda^{qp}(k)|, \tag{40}$$

and make use of Eq. (36) to cast the qp approximation (QPA) of the spectral function explicitly in the form of a Lorentzian

$$S_\Lambda^{qp}(k;\omega) = \frac{1}{\pi}\frac{z(k)\gamma(k)}{[\omega - \varepsilon_\Lambda^{qp}(k)]^2 + [\gamma(k)]^2}. \tag{41}$$

### C. Calculation of the *G* matrix

The calculation of the *G* matrix and the subsequent construction of the resulting self-energy will summarized in this subsection. A convenient basis for the determination of the *G* matrix is given by two-particle states with good total momentum, magnitude of the relative momentum, orbital angular momentum, total spin, and total angular momentum. Starting with states which have good momentum for the individual particles (and spin, etc.) the *G* matrix can be written as

$$\langle \boldsymbol{k}_3\boldsymbol{k}_4; Y_3N_4|G(\Omega)|\boldsymbol{k}_1\boldsymbol{k}_2; Y_1N_2\rangle = \langle \boldsymbol{k}_3\boldsymbol{k}_4; Y_3N_4|V|\boldsymbol{k}_1\boldsymbol{k}_2; Y_1N_2\rangle - \sum_{Y_5}\int\frac{d\omega_5}{2\pi i}\int\frac{d\boldsymbol{k}_5}{(2\pi)^3}\int\frac{d\boldsymbol{k}_6}{(2\pi)^3}\langle \boldsymbol{k}_3\boldsymbol{k}_4; Y_3N_4|V|\boldsymbol{k}_5\boldsymbol{k}_6; Y_5N_6\rangle$$
$$\times g_{Y_5}^{(0)}(\boldsymbol{k}_5;\omega_5)g_N^{(0)}(\boldsymbol{k}_6;\Omega-\omega_5)\langle \boldsymbol{k}_5\boldsymbol{k}_6; Y_5N_6|G(\Omega)|\boldsymbol{k}_1\boldsymbol{k}_2; Y_1N_2\rangle. \tag{42}$$

Each particle label corresponds to a momentum (spin and isopin) eigenstate with the convention that the leftmost states correspond to hyperons. The conserved total energy, $\Omega \equiv \omega_1 + \omega_2$, has been introduced in Eq. (42), and spin and isospin labels have been supressed for clarity. This equation may be simplified by performing the integral over $\omega_5$ for the propagator for the intermediate *YN* state:

$$g_{Y_5N}^{II}(\boldsymbol{k}_5,\boldsymbol{k}_6;\Omega) \equiv -\int\frac{d\omega_5}{2\pi i}g_{Y_5}^0(\boldsymbol{k}_5;\omega_5)g_{N_6}^0(\boldsymbol{k}_6;\Omega-\omega_5)$$
$$= \frac{\theta(|\boldsymbol{k}_6| - k_F)}{\Omega - \varepsilon_Y(\boldsymbol{k}_5) - \varepsilon_N(\boldsymbol{k}_6) + i\eta}. \tag{43}$$

Conservation of total momentum allows a change to total momentum,

$$\boldsymbol{Q} \equiv \boldsymbol{k}_1 + \boldsymbol{k}_2 = \boldsymbol{k}_3 + \boldsymbol{k}_4 = \boldsymbol{k}_5 + \boldsymbol{k}_6, \tag{44}$$

and relative momentum,

$$\boldsymbol{q}_i \equiv \left(\frac{\mu_Y}{m_Y}\right)\boldsymbol{k}_3 - \left(\frac{\mu_Y}{m_N}\right)\boldsymbol{k}_4, \tag{45}$$

$$\boldsymbol{q}_f \equiv \left(\frac{\mu_Y}{m_Y}\right)\boldsymbol{k}_1 - \left(\frac{\mu_Y}{m_N}\right)\boldsymbol{k}_2, \tag{46}$$

$$\boldsymbol{q}' \equiv \left(\frac{\mu_Y}{m_Y}\right)\boldsymbol{k}_5 - \left(\frac{\mu_Y}{m_N}\right)\boldsymbol{k}_6. \tag{47}$$

The reduced mass for the *YN* system has been introduced as

$$\mu_Y \equiv \frac{m_Y m_N}{m_Y + m_N}. \tag{48}$$

The *G* matrix integral equation now has the form

$$\langle \boldsymbol{q}_f; Y_3N_4|G(\boldsymbol{Q};\Omega)|\boldsymbol{q}_i; Y_1N_2\rangle = \langle \boldsymbol{q}_f; Y_3N_4|V|\boldsymbol{q}_i; Y_1N_2\rangle + \sum_{Y_5}\int\frac{d\boldsymbol{q}'}{(2\pi)^3}$$
$$\times\langle \boldsymbol{q}_f; Y_3N_4|V|\boldsymbol{q}'; Y_5N_6\rangle g_{Y_5N}^{II}(\boldsymbol{q}',\boldsymbol{Q};\Omega)\langle \boldsymbol{q}'; Y_5N_6|G(\boldsymbol{Q};\Omega)|\boldsymbol{q}_i; Y_1N_2\rangle. \tag{49}$$

In order to perform a partial-wave decomposition of the relative motion it is first necessary to eliminate the angular dependence in Eq. (43) since it couples different angular momentum states. This is accomplished by an angle-averaging procedure. The straightforward approach to angle-averaging leads to

$$\overline{g}_{YN}^{II}(q',Q;\Omega) \equiv \frac{1}{4\pi}\int d\Omega_{\hat{q}'}g_{YN}^{II}(\boldsymbol{q}',\boldsymbol{Q};\Omega), \tag{50}$$

for the angle-averaged propagator. This definition suffers from two problems. First, the integral in Eq. (50) cannot in general be performed analytically. More of a problem, however, is the fact that Eq. (50) no longer shares the simple analytic structure of the original propagator, Eq. (43). The prescription of Eq. (50) "smears" the simple pole, which creates problems later in the calculation of the *G* matrix. For this reason, angle-averaging is implemented in a different way. Instead of averaging the entire propagator at once, the numerator and denominator of Eq. (43) are angle-averaged separately. This leads to the new definition

$$\overline{g}_{YN}^{II}(q',Q;\Omega) \equiv \frac{\overline{\theta}(q',Q;k_F)}{\Omega - \overline{\varepsilon}_{YN}(q',Q;k_F) + i\eta} \tag{51}$$

which makes use of a shorthand notation for the two-particle energy,

$$\varepsilon_{YN}(\boldsymbol{q}',\boldsymbol{Q}) = \varepsilon_Y(\boldsymbol{q}',\boldsymbol{Q}) + \varepsilon_N(\boldsymbol{q}',\boldsymbol{Q}). \tag{52}$$

An additional simplification of

$$\overline{\varepsilon_B}(k_B) \equiv \varepsilon_B(\overline{k_B}), \tag{53}$$

is made, where the sp momentum is angle-averaged instead of the energy. The sp momenta $k_Y$ and $k_N$ can of course be obtained from $q'$ and $Q$. A dependence on $k_F$ arises because the Pauli restriction on allowed angles is taken into account even though the two parts of the propagator are angle-averaged separately. In practice, only a few terms in the partial-wave expansion make up the bulk of the contribution and the sum may be truncated to good approximation.

The NSC89 interaction possesses a strong tensor force which can couple states of different orbital angular momentum, $L$. The tensor force is primarily the result of pion exchange and is strongest for the $\Lambda N$-$\Sigma N$ channel. Pion exchange is nominally forbidden for the $\Lambda N$-$\Lambda N$ channel because isospin cannot be conserved at the $\Lambda\Lambda\pi$ vertex for a $\Lambda$ with zero isospin. Charge symmetry breaking voids this restriction to some extent, but the tensor force in this channel remains relatively weak. The strong interaction does not violate parity, so the $L$-values can only change by 0 or 2 units, since the total angular momentum is conserved and the total spin is restricted to 0 or 1. Under these conditions, it is possible to consider eigenstates of total angular momentum, $J = L + S$. In this basis, the $G$ matrix is given by

$$\begin{aligned}
&\langle k_f J(L_f S_f T); Y_3 N_4 | G(Q;\Omega) | k_i J(L_i S_i T); Y_1 N_2 \rangle \\
&\quad = \langle k_f J(L_f S_f T); Y_3 N_4 | V | k_i J(L_i S_i T); Y_1 N_2 \rangle \\
&\qquad + \sum_{Y_5 L' S'} \int dq' q'^2 \langle k_f J(L_f S_f T); Y_3 N_4 | V | q J(L' S' T); Y_5 N_6 \rangle \\
&\qquad \times \overline{g}_{II}^{Y'N}(q,Q;\Omega) \langle q J(L' S' T); Y_5 N_6 | G(Q;\Omega) \\
&\qquad \times | k_i J(L_i S_i T); Y_1 N_2 \rangle,
\end{aligned} \tag{54}$$

where a label for the total isospin, $T$, has been included for completeness. The operators which define the potential matrix elements are all scalars in $J$ and $T$. This means that the matrix elements defined by Eq. (54) are independent of $M_J$ and $M_T$.

The integral equation for the $G$ matrix is now in its final form for numerical solution. A standard method for solving such a one-dimensional integral equation is to discretize the integral and invert the resulting matrix equation [51]. The discrete momentum mesh must be chosen with some care, taking into consideration the $q'$-dependence of both the potential matrix elements and the angle-averaged two-particle propagator. The potential matrix elements are quite smooth functions of the relative momentum in all important partial wave channels. The strong short-range part of the $YN$ interaction couples low momentum states to intermediate states with very high momentum. As a result, it is necessary to choose a $q'$-mesh which adequately covers the high $q'$ region. The $q'$-dependence of the propagator arises from two sources. The Pauli $\theta$-function in the numerator serves mainly to cut off $q'$ below a minimum, $q'_{min}(Q)$, defined by

$$q'_{min}(Q) \equiv \begin{cases} k_F - \left(\dfrac{\mu_Y}{m_Y}\right) Q & \left(\dfrac{\mu_Y}{m_Y}\right) Q < k_F \\ 0 & \text{otherwise}. \end{cases} \tag{55}$$

For $\Omega$ above a certain threshhold, $\Omega_{min}(Q)$, there will be a pole in the angle-averaged propagator (Eq. (51)). This pole occurs for a value, $q'_0$, of the relative momentum defined by

$$\Omega = \overline{\varepsilon}_{YN}(q'_0, Q; k_F). \tag{56}$$

The pole location, $q'_0$, as well as the cutoff value, $q'_{min}$, are different for the two $YN$ channels. This means that separate $q'$-meshes must be constructed for each channel.

The $\Lambda$ self-energy is obtained from the $G$ matrix in the following way

$$\begin{aligned}
\Sigma_\Lambda(k_\Lambda;\omega) = \sum_J (2J+1) \int dQ\, Q^2 \int \frac{d\xi_Q}{2} \\
\times \langle q J(LS) T; \Lambda N | G(Q; \omega + \varepsilon_N(k_N)) \\
\times | q J(LS) T; \Lambda N \rangle \theta(k_F - k_N),
\end{aligned} \tag{57}$$

where the nucleon mean-field propagator was used. The relative momentum, $q$, and the nucleon momentum, $k_N$, are functions of the $\Lambda$ momentum, $k_\Lambda$, and the integration variables. The self-energy allows a new $\Lambda$-spectrum to be defined using Eq. (32). The new spectrum is used to define a new $\Lambda$-propagator according to Eq. (33) for input into Eq. (54) for the $G$ matrix. An essentially self-consistent spectrum is achieved after only a few iterations as discussed in the next section. With a consistent $\Lambda$-spectrum, the spectral function may be calculated as in Eq. (35). It should be noted that the spectral function is only defined for $\omega > \omega_{min}(k_\Lambda)$, and a meaningful spectral function can only be calculated for $k_\Lambda$ such that $\varepsilon^{qp}_\Lambda(k_\Lambda) > \omega_{min}(k_\Lambda)$. In practice, $\omega_{min}(k_\Lambda)$ depends on $k_\Lambda$, but in principle, $\omega_{min}(k_\Lambda) = \varepsilon^{qp}_\Lambda(0)$ for all $k_\Lambda$.

## III. RESULTS

The presentation in this section starts with a discussion of some of the qualitative features related to the spectral function and the self-energy. After this general discussion results will be presented for the spectral functions, the location of their peak, the magnitude of their width, and the strength contained in the peak. Comparisons with results for nucleon spectral functions will be made throughout. Of specific interest is the influence of the coupling to the $\Sigma N$ states on the $\Lambda$ self-energy and spectral function. This effect will be illustrated by comparing with results where this coupling has been eliminated.

### A. Qualitative features of the Λ spectral function and self-energy

From the definition of the spectral function in Eq. (10), the expression

$$a^\dagger_{\boldsymbol{k}} |\Psi(E_0)\rangle \tag{58}$$

has a physical interpretation as the state resulting from addition of a $\Lambda$ with quantum numbers, $\boldsymbol{k}$, to the NM ground

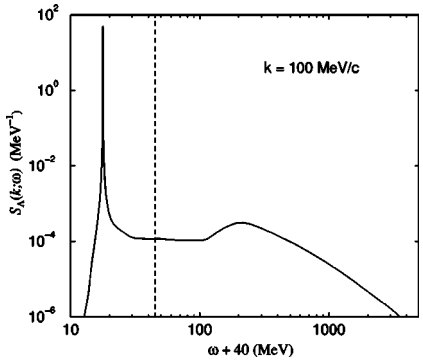


FIG. 3. Spectral function for a Λ with $k=100$ MeV/$c$. The vertical dashed line indicates the position of a delta-function spectral distribution for the limiting case of a free particle. Because of the 30 MeV binding for a Λ in nuclear matter, it is convenient to shift the horizontal axis by 40 MeV for plotting on a log scale.

state. By definition, this represents a product state of a Λ sp state and the correlated NM ground state. This will not be an eigenstate as long as there are Λ*N* interactions present in the Hamiltonian. The actual energy eigenstates of the composite system of a Λ in NM may be denoted by

$$|^{\Lambda}\Psi(E)\rangle. \tag{59}$$

The sp spectral function (see for example Fig. 3) involves the overlap between the simple physical state of Eq. (58) and the complicated eigenstate of Eq. (59) which includes all interactions between the Λ and the nuclear medium. The extent to which there is overlap illustrates how well the Λ sp state survives intact in the medium. For the case of no interactions between the Λ and the nucleons, the overlap is perfect, since the state of Eq. (58) is an eigenstate in this situation. This is evidenced by the $\delta$ function spectral distribution appropriate for a free particle, as indicated by a dashed line at the kinetic energy in Fig. 3. Interactions between the Λ and nucleons are responsible for the transition from the simple $\delta$ function structure to the more complex distribution of sp strength realized in NM. The mechanism behind the spreading of sp strength can be understood as the mixing of a sp state at a given energy with two-particle one-hole ($2p$-$1h$) states which span a continuum of energies. This is graphically illustrated in Fig. 4 where part a) identifies the noninteracting Λ and part b) shows the interaction that couples this state to the available $2p$-$1h$ states. Although the sp state is no longer an eigenstate of the many-body Hamiltonian, its quantum numbers are still conserved by the interaction. The total strength associated with the original sp state, though fragmented, is fixed. This is reflected in the sum rule of Eq. (11). Details of the strength distribution are determined by the density of $2p$-$1h$ states which increases with energy and the strength with which the interaction couples these states to the unperturbed sp state. This information is summarized in the imaginary part of the self-energy, shown for example in Fig. 5. Note that the decomposition in partial wave contributions emphasizes the dominance of the $^3S_1$ channel.

From Eq. (28), the imaginary part of the self-energy may be written as

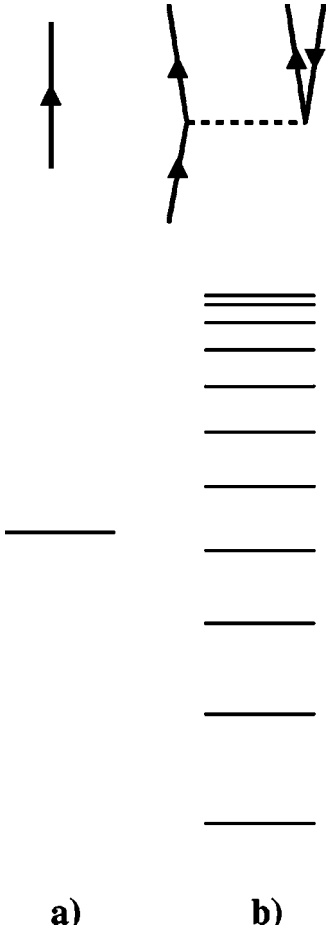


FIG. 4. In part (a) a free Λ occupies a sp state at a fixed energy. Part (b) displays the Λ*N* interaction which permits coupling to intermediate $2p$-$1h$ states which span a range of energies, the density of states increasing with energy as schematically shown.

$$\mathrm{Im}\,\Sigma_\Lambda(k,\omega) \propto \sum_{k'<k_F} \mathrm{Im}\langle kk'|G(\omega+\varepsilon_N(k'))|kk'\rangle, \tag{60}$$

where the nucleon hole spectral function has been replaced by the corresponding mean-field form given by Eq. (8). It

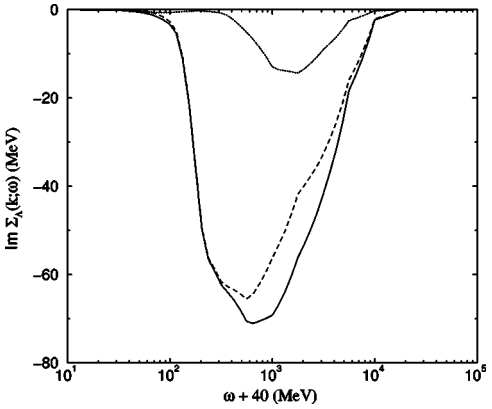


FIG. 5. Imaginary part of the Λ self-energy for $k=100$ MeV/$c$. The broken curves represent contributions to the overall self-energy from the $^3S_1$ (dash) and $^1S_0$ (dot) partial wave channels.

can be shown [52] in turn that the imaginary part of the $G$ matrix may be expressed in terms of the uncorrelated two-particle propagator as

$$\mathrm{Im}\,\langle kk'|G(\Omega)|kk'\rangle \propto \sum_{k_1k_2} |\langle kk'|G(\Omega)|k_1k_2\rangle|^2 \times \mathrm{Im}\, g^{II}_{unc}(k_1k_2;\Omega). \quad (61)$$

The imaginary part of the uncorrelated $\Lambda N$ propagator is proportional to the diagonal spectral density [see Eq. (24)]

$$\mathrm{Im}\, g^{II}_{unc}(k_1k_2;\Omega) \propto S^{II}_{unc}(k_1k_2;\Omega). \quad (62)$$

If particles in the intermediate state are not dressed by interactions with the medium (as they would be in a fully self-consistent calculation), but rather are treated as mean-field particles, then

$$S^{II}_{unc}(k_1k_2;\Omega) \rightarrow \delta(\Omega - \varepsilon_{2p}(k_1k_2))\,\theta(k_2 - k_F) \quad (63)$$

and the two-particle spectral function reduces to a delta-function which picks out states with total energy, $\Omega$. In this simplified case, Eq. (60) becomes

$$\mathrm{Im}\,\Sigma_\Lambda(k,\omega) \propto \sum_{k'<k_F}\sum_{k_1}\sum_{k_2>k_F} |\langle k_1k_2|G(\Omega)|kk'\rangle|^2 \times \delta(\omega - \varepsilon_{2p1h})\,\delta_{k,k_1+k_2-k'}, \quad (64)$$

where

$$\varepsilon_{2p1h} \equiv \varepsilon_Y(k_1) + \varepsilon_N(k_2) - \varepsilon_N(k'), \quad (65)$$

and momentum conservation is indicated by the Kronecker symbol. Equation (64) reveals the direct connection between $\mathrm{Im}\,\Sigma_\Lambda(k,\omega)$ and the phase-space for $2p$-$1h$ states with momentum, $k$, and energy, $\omega$. Aside from the weighting provided by the $G$ matrix elements, the imaginary part of the self-energy is directly proportional to the available $2p$-$1h$ phase-space. The correlations present between particles in the intermediate state will make the spectral function more complicated than Eq. (63) for the uncorrelated case and typically leads to a diminished density of states at low energy [53]. However, this does not substantially alter the physical interpretation of $\mathrm{Im}\,\Sigma_\Lambda$ as expressed in Eq. (64). The imaginary part of the self-energy is still proportional to a weighted $2p$-$1h$ phase space but the intermediate particles are better thought of as quasiparticles carrying reduced strength.

### *Coupling 1p to 2p-1h states*

The $\delta$-functions in Eq. (64) permit the integrals over intermediate state variables to be performed explicitly. Taken together with Eq. (60), an expression is readily derived for Im $G$ where phase-space factors are conveniently decoupled from the weighting matrix elements,

$$\mathrm{Im}\,\langle p|G(Q,\Omega)|p\rangle = -\pi \sum_{YL} |\langle p|G(Q,\Omega)|q_0\rangle|^2 \times \underbrace{Q_{YN}(Q,q_0)q_0^2\left|\frac{\partial\,\varepsilon_{YN}}{\partial\, q}\right|^{-1}_{q=q_0}}_{\simeq\sqrt{\Omega}\simeq q_0}. \quad (66)$$

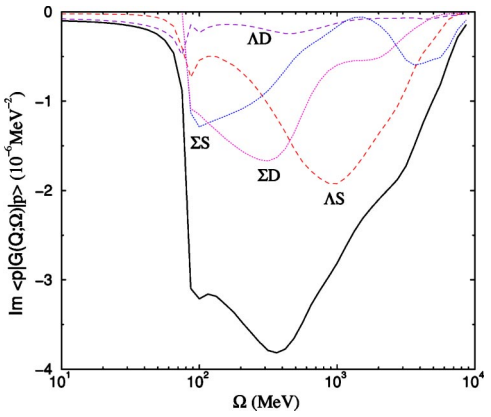


FIG. 6. (Color online) The components of Im $G$ as defined by Eq. (66). One curve is associated with each $YN$ intermediate state accessible from the initial $\Lambda N\ ^3S_1$ state. The full curve is the sum of the four components.

Here $p$, $Q$ and $\Omega$ are the relative momentum, total momentum and total energy for the $\Lambda N$ state obtained by averaging over the nucleon hole momentum. The on-shell relative momentum, $q_0$, is defined by the two-particle energy through

$$\Omega \equiv \varepsilon_{YN}(Q,q_0), \quad (67)$$

and varies depending on which hyperon ($\Lambda$ or $\Sigma$) is present in the intermediate state. In the following we will study the contributions to Eq. (66) which in turn through Eq. (60) determine the $\Lambda$ self-energy.

As indicated in Eq. (66), there are two sources of energy dependence for diagonal matrix-elements of Im $G$. There is a phase-space factor which, aside from Pauli effects and deviations from free spectra for the intermediate particles, contributes a simple, structureless energy dependence for each $YN$ channel. The two $YN$ channels do possess different energy thresholds and this does lead to an expectation of structure at the $\Sigma N$ threshold (region near 70 MeV in Fig. 6) purely on the basis of phase-space considerations. However, most structure found in the energy dependence of Im $G$ can be attributed to the half-on-shell matrix elements of $G$ which effectively couple the $1p$ and $2p$-$1h$ states.

Taking the example of an initial $\Lambda N\ ^3S_1$ state, Eq. (66) is plotted in Fig. 6. Contributions from each of four possible intermediate states, characterized by different YL combinations, are plotted together with their sum. All terms contribute significantly except for the $\Lambda N\ ^3D_1$ intermediate state which couples relatively weakly to the initial state.

Though the form of Eq. (66) is useful for isolating purely phase-space influences on the energy dependence of Im $G$, a complex, non-linear tangling of states remains concealed within the half-on-shell $G$ matrix elements. These tangled intermediate states can be further unscrambled by considering a dissection of the pertinent $G$ matrix elements into a pair of complementary approximations. One may define a "direct" approximation to a particular matrix element, $\langle\alpha|G|\beta\rangle$, by eliminating all matrix elements $\langle\gamma|V|\delta\rangle$ from the definition of the $G$ matrix equation *except* those where $\alpha=\gamma$ and $\beta=\delta$. The quantum numbers $\alpha,\beta,\gamma$ and $\delta$ here refer to the

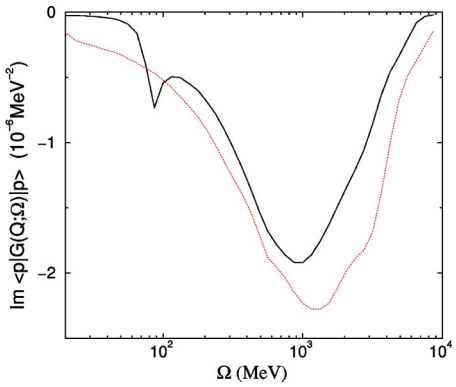


FIG. 7. (Color online) Dashed curve is the direct approximation to Im $G$ for the $\Lambda N\ ^3S_1$ intermediate state. The full curve is the Im $G$ component attributed to this same intermediate state when all couplings are intact. Note that there is no indirect contribution for this channel because the direct $\Lambda N\ ^3S_1 \rightarrow \Lambda N\ ^3S_1$ transition turns out to be crucial for the numerical determination of the $G$-matrix.

appropriate channels, for example $\Lambda N\ ^3S_1$, etc. The complementary "indirect" approximation to $G$ is defined by eliminating *only* those matrix elements of $V$ where $\alpha=\gamma$ and $\beta=\delta$. Note that complementary sets of approximate $G$ matrices are defined for each choice of initial and intermediate state.

As an example, consider the situation where only transitions to an intermediate $\Lambda N\ ^3S_1$ state are allowed. This can be accomplished by generating a new $G$ matrix where all matrix elements of $V$ are set to zero, except those which connect the intial state to the $\Lambda N\ ^3S_1$ intermediate state. In this case there is only a single term in the sum of Eq. (66), corresponding to the lone available intermediate state. This version of Im $G$, where only the direct route to the $\Lambda N\ ^3S_1$ intermediate state is available, is compared with the corresponding $\Lambda N\ ^3S_1$ term from the result for the fully correlated $G$-matrix in Fig. 7. The shapes are very similar except in the energy range near the $\Sigma N$ threshold and below. This similarity indicates that the effective couplings to the $\Lambda N\ ^3S_1$ intermediate state are only modestly influenced by the presence of the other intermediates, except in the vicinity of the $\Sigma N$ threshhold.

The $\Lambda N\ ^3S_1 - \Sigma N\ ^3D_1$ effective interaction is likewise dominated by direct coupling as shown in Fig. 8. This clearly shows that an energy region can be identified with states that are reached primarily via a tensor interaction (the few hundred MeV range). Contrast this with Fig. 7 where the $\Lambda N\ ^3S_1 - \Lambda N\ ^3S_1$ term has no tensor interaction and peaks above 1 GeV. Indirect contributions therefore factor in only marginally.

For some channels, a direct approximation is not feasible. In these cases, turning off the direct $\Lambda N\ ^3S_1 - \Lambda N\ ^3S_1$ transition causes the numerical determination of the coupled channel $G$ matrix to become unstable. It still turns out to be useful to define and utilize a semi-direct approximation in these cases. In this approximation, the $\Lambda N\ ^3S_1 - \Lambda N\ ^3S_1$ potential is retained, along with the matrix elements for the direct transition. Inclusion of these matrix elements serves to stablize the numerics while only interfering minimally (at higher order). A semi-direct approximation to $\Lambda N\ ^3S_1 - \Sigma N\ ^3S_1$ channel involves turning off all tensor interactions and leaving only the two central transitions. Figure 9 confirms that this approximation primarily cuts in the "tensor" region identified from Fig. 8 and this is where the indirect approximation gives its largest contribution.

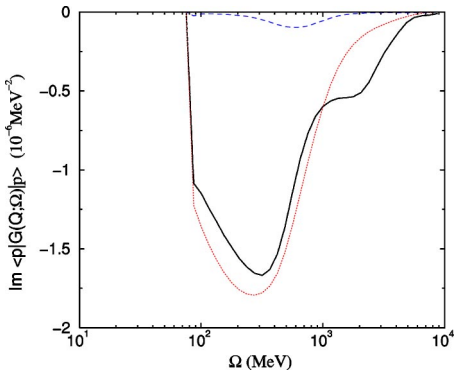


FIG. 8. (Color online) Direct (dotted) and indirect (dashed) approximations to Im $G$ for the $\Sigma N\ ^3D_1$ intermediate state.

### B. The quasi-particle peak

As indicated by the spectral function peak in Fig. 3, an energy region with a substantial amount of sp strength survives the mixing with the $2p$-$1h$ states. However, this qp peak is shifted in energy, broadened and has lost some fraction of strength compared to the delta-function distribution appropriate for a non-interacting particle.

#### *1. Location*

The location of the peak is given by the qp energy as defined in Eq. (36). The real part of the self-energy, playing the role of a sp potential, shifts the peak from its unperturbed location at the kinetic energy. The self-energy can be split into two pieces,

$$\Sigma_\Lambda(k;\omega) = \Sigma_V^\Lambda(k) + \Sigma_\Delta^\Lambda(k;\omega), \tag{68}$$

each corresponding to a different type of physical process as indicated in Fig. 10. Treating the self-energy at lowest order in the $\Lambda N$ interaction (the HF approximation) only elastic

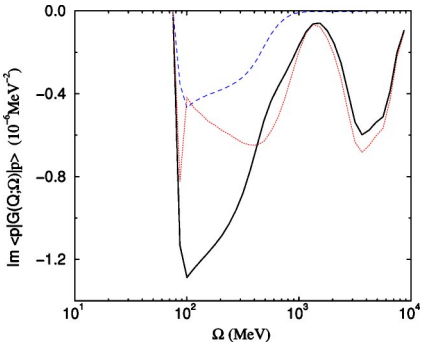


FIG. 9. (Color online) Semi-direct (dotted) and indirect (dashed) approximations to Im $G$ for the $\Sigma N\ ^3S_1$ intermediate state. Semi-direct because the $\Lambda N\ ^3S_1 - \Lambda N\ ^3S_1$ couplings must still be included in order to obtain reasonable results.

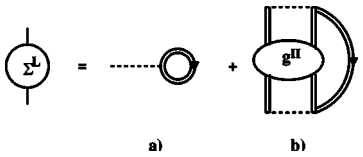


FIG. 10. In part a) the HF part of the self-energy is shown. Part b) includes the coupling to intermediate $2p$-$1h$ states. This contribution corresponds to the second term in Fig. 1(b) for the ladder equation.

scattering between the lambda and nucleons below the Fermi energy is considered as illustrated in Fig. 10(a). This leads to a real, energy-independent contribution to the self-energy, $\Sigma_V^\Lambda(k)$. This term is relatively large and positive, on the order of 50 MeV, reflecting the repulsive character of the bare interaction.

The coupling to $2p$-$1h$ intermediate states is represented by the diagram of Fig. 10(b). Such processes induce a complex, energy-dependent component to the self-energy, $\Sigma_\Delta^\Lambda(k;\omega)$. This self-energy piece obeys a dispersion relation [see Eq. (29)],

$$\mathrm{Re}\,\Sigma_\Delta^\Lambda(k;\omega) = \frac{-P}{\pi}\int_{\varepsilon_T^\Lambda}^{\infty} d\omega' \frac{\mathrm{Im}\,\Sigma_\Lambda(k;\omega')}{\omega-\omega'}. \tag{69}$$

This means that the real part of the self-energy in the neighborhood of some particular energy, such as $\varepsilon_\Lambda^{qp}$, requires knowledge of $\mathrm{Im}\,\Sigma_\Lambda(k;\omega)$ at all energies. The imaginary part of the self-energy is dominated by a broad, smooth peak at high energy, as seen in Fig. 5. In contrast, the qp peak resides at a much lower energy, $\varepsilon_\Lambda^{qp}(k)$; far removed from the bulk of the strength in $\mathrm{Im}\,\Sigma_\Lambda(k;\omega)$, which is centered at some energy, $\omega_0$, in the GeV range. If the only appreciable contribution to Eq. (69) evaluated at $\omega=\varepsilon_\Lambda^{qp}(k)$ comes from $\omega'$ near $\omega_0$, then the denominator in the integrand may be approximated as a constant: $\varepsilon_\Lambda^{qp}(k)-\omega_0$. This leaves

$$\begin{aligned}\mathrm{Re}\,\Sigma_\Delta^\Lambda(k;\varepsilon_\Lambda^{qp}(k)) &\simeq \frac{-1}{\pi}\frac{1}{\varepsilon_\Lambda^{qp}(k)-\omega_0}\int_{\varepsilon_T^\Lambda}^{\infty} d\omega'\,\mathrm{Im}\,\Sigma_\Lambda(k;\omega') \\ &= \frac{-1}{\pi}\frac{I_0}{\varepsilon_\Lambda^{qp}(k)-\omega_0},\end{aligned} \tag{70}$$

where $I_0$ is just the integrated strength in $\mathrm{Im}\,\Sigma_\Lambda(k;\omega)$. In this approximation $\mathrm{Re}\,\Sigma_\Delta^\Lambda(k;\varepsilon_\Lambda^{qp}(k))$ depends on only two parameters which together characterize the gross properties of $\mathrm{Im}\,\Sigma_\Lambda(k;\omega)$; the integrated strength, $I_0$, and the centroid of the high-energy peak, $\omega_0$. Though nominally $k$ dependent, the parameters $I_0$ and $\omega_0$ should vary only slowly with $k$ since they characterize the gross structure of $\mathrm{Im}\,\Sigma_\Lambda(k;\omega)$ at high energy; structure which is far removed from the low-energy realm of the qp peak. These two parameters define a model for a simple low-energy approximation to $\mathrm{Re}\,\Sigma_\Delta^\Lambda$,

$$\mathrm{Re}\,\Sigma_\Delta^{\Lambda,\mathrm{model}}(k;\varepsilon_\Lambda^{qp}(k)) \equiv \frac{-1}{\pi}\frac{I_0}{\varepsilon_\Lambda^{qp}(k)-\omega_0}. \tag{71}$$

The full structure of the self-energy is shown in Fig. 11 with the two-parameter model for comparison.

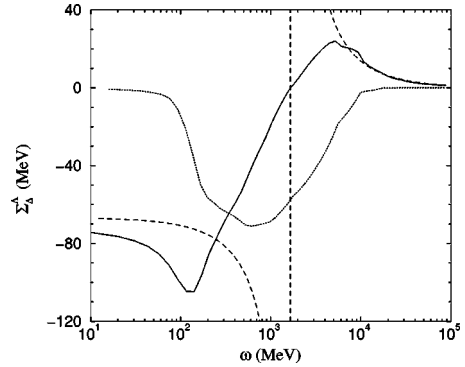


FIG. 11. Real and imaginary parts of the exact self-energy are plotted with the solid lines and the real part from the model is plotted as a dashed curve for comparison.

Decreasing the density of $2p$-$1h$ states and/or the strength of coupling to these states is analogous to a decrease in the parameter $I_0$. This simply scales down the real part of the self-energy for all energies, thereby reducing the binding contribution to $\varepsilon_\Lambda^{qp}$. Alternatively, moving the $2p$-$1h$ states to higher energy can be mimicked by an increase in the parameter $\omega_0$, which likewise results in a reduction in the real part of the self-energy at $\varepsilon_\Lambda^{qp}$ and a consequent decrease in qp binding.

The success of this simple model, limited as it is, indicates that $\varepsilon_\Lambda^{qp}$ is dominantly determined by high-energy $2p$-$1h$ states, but at the same time is relatively insensitive to details of the coupling to these states. To quantify the insensitivity of $\varepsilon_\Lambda^{qp}$ to low-lying excited states, one can isolate the low-energy tail of $\mathrm{Im}\,\Sigma_\Lambda(k;\omega)$ in Eq. (69), and examine its effect on $\varepsilon_\Lambda^{qp}$. The first 100 MeV of $\mathrm{Im}\,\Sigma_\Lambda(k;\omega)$ above the lambda threshold only contributes to $\varepsilon_\Lambda^{qp}$ at the level of a few percent. The disparity of about 10 MeV between the model and the full result can be attributed to the finite width of the peak, and especially the low-energy shoulder in the range of a few 100 MeV where coupling to the $\Sigma N$ channel is most important. It should be noted that these results are contingent on $\mathrm{Im}\,\Sigma_\Lambda(k;\omega)$ being of a form similar to that depicted in Fig. 5. The imaginary part of the self-energy is dominated by its structure at high energy precisely when SRC dominate the $\Lambda N$ effective interaction from which it is derived. This depends in part on the short-range behavior of the bare interaction, but also on the approximation method selected when defining the effective interaction. The ladder approximation adopted in this work is specifically chosen because it incorporates the essential features of SRC while de-emphasizing LR behavior and more collective states which naturally occur at low excitation energy. A realistic calculation for a finite hypernucleus, utilizing the same bare interaction, but going beyond the ladder approximation might well show greater sensitivity to low-lying states [10,14,16].

Since $I_0<0$, the real part of the self-energy will be negative for any energy below $\omega_0$, including the "on-shell" region near the qp peak. This means that the self-energy term which represents the coupling to high-energy $2p$-$1h$ states [Fig. 10(b)] will always lower the energy of the qp state. This result is familiar from perturbation theory, where a second-order correction to the energy always serves to lower the

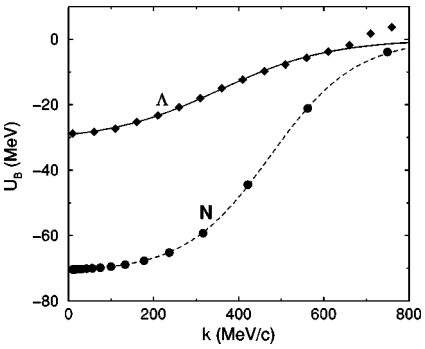


FIG. 12. Potentials of Wood-Saxon form are fitted to calculated data for the Λ and the nucleon, identified by diamonds and circles, respectively. The analytic approximation is useful when the derivative of a particle spectrum is required.

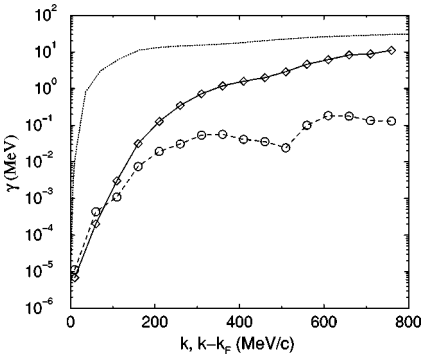


FIG. 13. The curve marked by diamonds represents the qp width as a function of $k$. The curve with circles represents an approximation to the width based on the local density of $2p$-$1h$ states. The dotted curve represents the corresponding widths for nucleons as a function of $k-k_F$.

energy of the ground state. This binding more than offsets the HF contribution to $\varepsilon_\Lambda^{qp}$ and leads to a monotonically increasing qp spectrum. A sp potential, $U_\Lambda(k)$, defined by

$$\varepsilon_\Lambda^{qp}(k) \equiv t_\Lambda(k) + U_\Lambda(k), \tag{72}$$

is plotted in Fig. 12 together with the sp potential employed for the nucleons.

The net binding of 30 MeV for a lambda at rest in NM is consistent with other calculations [4] as well as an extrapolation from experimentally measured $s$-shell binding energies for hypernuclei [54]. Only the $S$-waves (including the tensor-coupled channels) are considered in this work. Higher partial waves yield corrections to $\varepsilon_\Lambda^{qp}$ on the order of no more than 10% and even at this level tend to cancel each other out [17].

#### *2. Width*

In contrast to the position of the qp peak, which is essentially determined by the structure of the imaginary part of the self-energy at very high energies, the width of the peak is directly proportional to the local value of Im $\Sigma_\Lambda$ at the qp energy [Eq. (40)]. To the extent that coupling to these low-lying $2p$-$1h$ states is only weakly momentum dependent (for low values of $k$), the width is directly proportional to the local density of $2p$-$1h$ states. Phase space restrictions near the $2p$-$1h$ threshold determine the low-energy structure of the imaginary part of the self-energy [55] according to

$$\mathrm{Im}\,\Sigma_\Lambda(k;\omega) \simeq c(k)[\omega - \varepsilon_T^\Lambda]^2, \quad \omega \to \varepsilon_T^\Lambda. \tag{73}$$

For values of $k$ such that $\varepsilon_\Lambda^{qp}(k)$ is low enough to fall in the energy range where Eq. (73) is valid, the qp width can be simply expressed as a function of the peak position,

$$\gamma(k) \simeq c'(k)[\varepsilon_\Lambda^{qp}(k) - \varepsilon_T^\Lambda]^2. \tag{74}$$

This approximation is shown together with the calculated width as a function of momentum in Fig. 13, where the factor $c'(k)$ has been approximated as a constant, independent of $k$. Although this model for the qp width is not precisely accurate except very near $k=0$, it does suggest the origin of the growth of $\gamma(k)$ with increasing $k$. For comparison, the corresponding results for nucleons are also included in Fig. 13 as the dotted curve plotted as a function of $k-k_F$, using the results of Ref. [39]. Especially at small momenta above the particle thresholds, the nucleon width is several orders of magnitude larger than the Λ one, suggesting that the $NN$ interaction generates a much stronger coupling to the low-lying $2p$-$1h$ states than the $YN$ one. At higher momenta, this difference is reduced to about a factor of 3.

If the qp part of the spectral function is interpreted as a distinct sp-like state, then $\gamma_{qp}(k)$ is the width induced by coupling to a population of nearby states. Overlaying the QPA to the spectral function on top of the full spectral function, Fig. 14, demonstrates the utility of the QPA for low $k$. A sharp rise in Im $\Sigma_\Lambda(k;\omega)$ occurs in the vicinity of $\omega \simeq 200$ MeV as can be seen in Fig. 5. When $\varepsilon_\Lambda^{qp}(k)$ reaches this energy range, the QPA is no longer a reasonable approximation. This occurs for a Λ with momentum in the neighborhood of $k \simeq 600$ MeV/$c$ and is a sign that another energy threshold has been crossed. This threshold is discussed in Sec. III C.

#### *3. Strength*

According to Eq. (39), the amount of spectral strength concentrated in the qp peak is given by the derivative of Re $\Sigma_\Delta^\Lambda(k;\omega)$ with respect to $\omega$ locally at $\varepsilon_\Lambda^{qp}$. In terms of the dispersion relation for Re $\Sigma_\Delta^\Lambda(k;\omega)$, Eq. (39) becomes

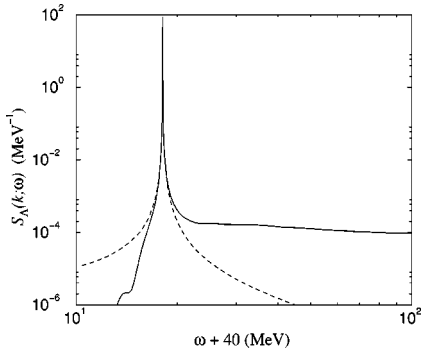


FIG. 14. Solid curve is the full spectral function for $k = 110$ MeV/$c$. The dashed curve is the QPA.

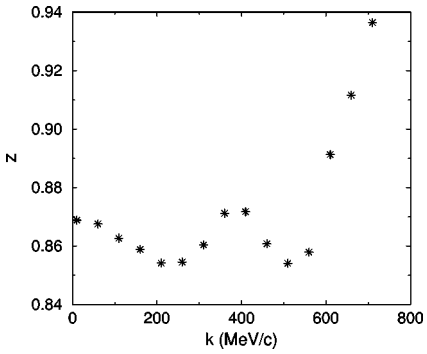


FIG. 15. Quasi-particle strength as a function of $k$.

$$z(k) = \left[ 1 - \frac{P}{\pi} \int_{\varepsilon_F}^{\infty} d\omega' \frac{\mathrm{Im}\,\Sigma_\Lambda(k;\omega')}{(\varepsilon_\Lambda^{qp}(k) - \omega')^2} \right]^{-1}. \qquad (75)$$

Comparing to Eq. (29), the strength in the qp peak, $z(k)$, is seen to exhibit a greater sensitivity to the structure of $\mathrm{Im}\,\Sigma_\Lambda(k;\omega)$ than does the peak position, $\varepsilon_\Lambda^{qp}$. The $z$-factor (Fig. 15) is most accurate as a measure of strength in the peak of the spectral function for low values of $k$.

A nuclear matter calculation for nucleons similar to this one [37] yields a particle spectral function shown in Fig. 16, for a momentum just above $k_F$. The $z$-factor obtained from this calculation is $z_N(k_F)=0.72$, which is substantially reduced compared to $z_\Lambda(0)=0.87$ for a similar $\Lambda$ qp state. These two momentum values are compared because each qp sits at the lowest possible excitation energy for a qp in the respective systems. In Ref. [37], the depletion of the qp strength is explained in terms of couplings to $2h$-$1p$ states, which moves approximately 10% of the sp strength to energies below $\varepsilon_F$, and coupling to $2p$-$1h$ states, which distributes another 18% to higher energies in the particle domain. The corresponding fraction of sp strength in the particle domain is 13% for the lambda, compared to 18% for nucleons. A more detailed look at the distribution of strength as a function of energy is given in Fig. 17. This figure displays for four different momenta the fraction of the sp strength that is recovered as a function of energy by intergating this strength up to that energy. This figure shows that most of the strength is accounted for at energies corresponding to 2 GeV. In the case of nucleons interacting by means of the Reid interaction the strength has to be gathered up to energies of 10 GeV [37] illustrating the harder core of this interaction.

The relative effects of tensor and short-range correlations can be untangled to some extent. Turning off the $^3S_1 - {}^3D_1$ tensor coupling in the Reid potential for nucleons indicates that this interaction is responsible for depleting the qp strength by about 6.5%, almost all within 1000 MeV of $\varepsilon_F$ [37]. Similarly, turning off the $\Lambda N$-$\Sigma N$ coupling in the NSC89 potential reveals that tensor effects are responsible for almost half of the reduction in the $\Lambda$ qp strength. A value of $z_\Lambda(0)=0.94$ is obtained when coupling to $\Sigma N$ states is cut off.

### C. The $\Sigma N$ Threshold

The effects associated with the inclusion of the $\Sigma N$ channel are illustrated in Figs. 18 and 19. In NM the $\Sigma N$ threshold opens at an energy about 90 MeV above the self-consistently determined $\Lambda N$ threshold. The mass difference is $m_\Sigma - m_\Lambda = 77$ MeV, but the $\Lambda$ is bound in NM by about 30 MeV whereas the $\Sigma$ binding is about half as much. Again, the imaginary part of the self-energy provides a picture of how the $\Sigma NN^{-1}$ $2p$-$1h$ states influence $\Lambda$ sp properties. The imaginary part of the self-energy is plotted in Fig. 18 for the case where coupling to the $\Sigma N$ states is turned off.

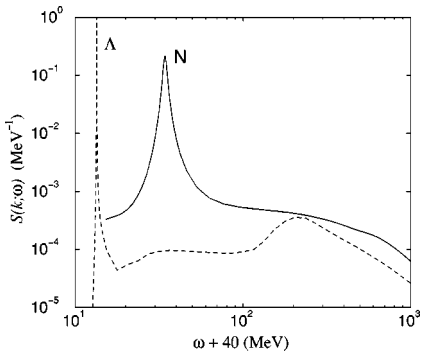


FIG. 16. Nucleon particle spectral function (solid) for $k=316$ MeV/$c$ with lambda spectral function (dashed) at $k=60$ MeV/$c$ for comparison.

Turning off the $\Sigma N$ coupling leads to a recovery of 7% of the strength in the qp peak as the $z$-factor increases from 0.86 to 0.93. A reduction in spectral strength is observed at all energies, but is particularly apparent at, and just above, the $\Sigma N$ threshold. There are two reasons $\Sigma NN^{-1}$ $2p$-$1h$ states are most influential in this energy region. First, a "threshold effect" is responsible for the sharp cusp in $\mathrm{Im}\,\Sigma_\Lambda$ near 100 MeV. This behavior may be understood physically in the same way as the cusp observed in the $\Sigma N$ elastic scattering cross-section [56]. In scattering theory, the elastic cross-section may be calculated from the bare two-body interaction via the on-shell elements of the $T$-matrix. In NM, an effective interaction, such as the $G$-Matrix is a generalization of the free-space $T$ matrix. Structure arises in the $\Lambda N$ $G$ matrix as a consequence of the strong coupling to the nearby $\Sigma N$ channel [57]. From Eq. (28), the imaginary part of the self-energy shares the same structure as the imaginary part of the $G$ matrix.

Second, isospin conservation in the strong $\Lambda N$ interaction forbids excitation of nuclear ph states via $\pi$-exchange. How-

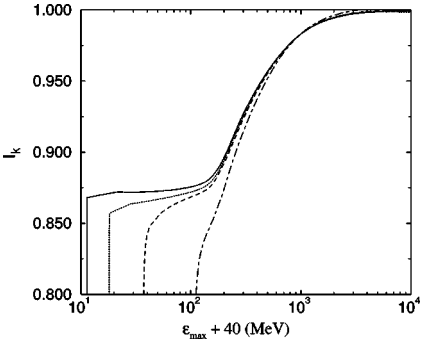


FIG. 17. Single-particle strength integrated from $\varepsilon_T^\Lambda$ to $\varepsilon_{max}$ as a function of $\varepsilon_{max}$ for different momenta. $k=10$ MeV (solid), $k=110$ MeV (dot), $k=210$ MeV (dash), $k=310$ MeV (dot-dash).

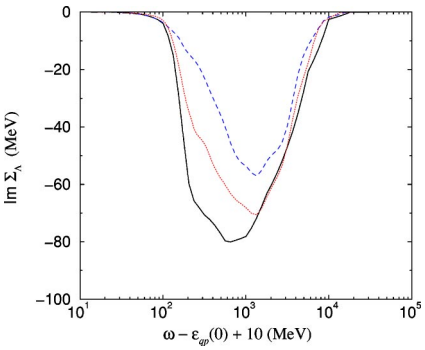


FIG. 18. (Color online) Im $\Sigma_\Lambda$ for the case where $\Lambda N$-$\Sigma N$ coupling is included (solid curve), without coupling (dashed) and when $\pi$-exchange is turned off in $V$ (dotted). Plotting with respect to self-consistently determined $\Lambda$ threshold energy ensures that the $\Sigma N$ threshold is in the same location for each curve. The value of the momentum in this plot corresponds to $k=10$ MeV/$c$.

ever, this is a strongly allowed process for the $\Sigma N$ interaction, preferentially exciting $\Sigma N N^{-1}$ $2p$-$1h$ states in the energy range of a few hundred MeV. Turning off the $\pi$-exchange component of the bare interaction (Fig. 18) demonstrates that it is partly responsible for the $\Sigma N$ channel's influence on the $\Lambda$, but apparently the non-tensor part of the $\Lambda N$-$\Sigma N$ coupling plays just as significant a role, even in the "tensor" region. The nucleon spectral function manifests a similar feature in the energy range dominated by the tensor interaction [39]. For nucleons the influence of the tensor force on the distribution of the sp strength corresponds to moving a similar amount of strength away from the peak as the amount corresponding to the effect of SRC [37].

The effect on the spectral function is to induce additional structure in the vicinity of the threshold energy (Fig. 19). The spectral signature of this new channel is a reduction of strength just below threshold followed by an enhancement immediately above threshold which slowly dies out at increasing energy. The location of the $\Sigma N$ threshold is dependent on the total momentum of the $\Lambda N$ pair. The self-energy involves an average over all values of $Q$ that can be realized for a $\Lambda$ with a given momentum, $k$, and a nucleon hole which can have a range of momentum according to the nuclear

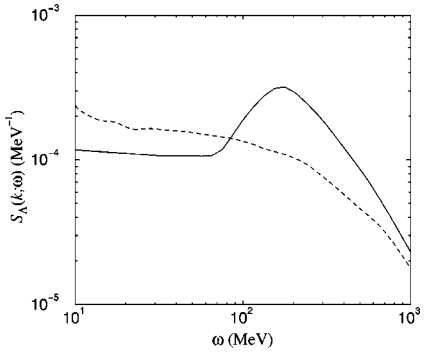


FIG. 19. Spectral function in the vicinity of the $\Sigma N$ threshold with $\Lambda N$-$\Sigma N$ coupling (solid) and without (dashed). Note that the $\Lambda$ threshold differs by about 30 MeV between the two cases. The momentum value in this example corresponds to $k \approx 100$ MeV/$c$.

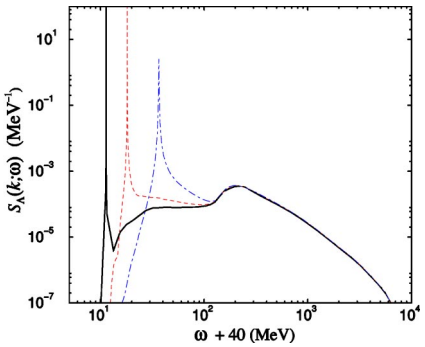


FIG. 20. (Color online) Spectral function for three values of $k_\Lambda$ show the $k$-independence of the high energy tail for $k=10$ MeV/$c$ (solid curve), 110 MeV/$c$ (dashed), and 210 MeV/$c$ (dash-dot).

density. This averaging smears out the location of the "cusp" structure in the self-energy and in the spectral function.

### D. The high-energy region

Away from the qp peak, at high-energy, the size and structure of the spectral function is primarily determined by two factors. The density of $2p$-$1h$ states increases like $\omega^{1/2}$ at high energy. This growth in spectral strength with energy is moderated by the strength of the coupling to these high energy states. A lambda with a reasonably low momentum couples to a nucleon hole state only with a low relative momentum. The high-energy $\Lambda N$ two-particle states couple most strongly to high relative momentum and the strength of the potential matrix elements between these two states depends on the short-range characteristics of the two-body interaction. A harder core allows a stronger coupling between states and correspondingly more spectral strength at high energy (see the following paragraph). The fact that structure in the high-energy region of the spectral function is primarily determined by the short-range behavior of the two-body interaction should be tempered by the knowledge that the short-range part of baryon-baryon interactions are poorly known. Typical potentials are designed, within whatever model, to fit only low-energy experimental data which does little to constrain the details of the repulsive core. This situation can be taken in two ways. On the one hand, the high-energy tail of the spectral function is just as uncertain in detail as the core of the interaction from which it is derived. On the other hand, it is also just as experimentally inaccessible and any observable which can be related to the detail of the tail in the spectral strength distribution could be used to gain insight into the behavior of the bare two-body interaction at short-range. In Fig. 20 the similarities of the tail of the spectral strength for different momenta is illustrated.

*Sum rule*. There exists a sum rule relating the energy-weighted integral of the spectral function to the matrix elements of $V$ in a very direct manner [58]. Writing the result from Ref. [58] for the case of a $\Lambda$ in NM,

$$\int_{\varepsilon_F}^{\infty} d\omega\ \omega S_p^\Lambda(k;\omega) = \frac{k^2}{2m_\Lambda} + \frac{1}{(2\pi)^3}\int d^3k' n_h(k')\langle \vec{k}\vec{k}'|V|\vec{k}\vec{k}'\rangle, \tag{76}$$

where $n_h(k)$ is the occupation probability of the sp nucleon state with momentum $k$,

$$n_h(k) = \int_{-\infty}^{\varepsilon_F} d\omega S_h^N(k,\omega). \tag{77}$$

Note that the two terms comprising the right-hand side of Eq. (76) are just the kinetic energy, $t_\Lambda(k)$, and the energy independent part of the self-energy, $\Sigma_V^\Lambda(k)$, respectively. The left-hand side of Eq. (76) may be formally divided into two pieces,

$$\int d\omega\ \omega S_p^\Lambda(k;\omega) \equiv \int d\omega\ \omega S_{qp}^\Lambda(k;\omega) + \int d\omega\ \omega S_{tail}^\Lambda(k;\omega), \tag{78}$$

the first corresponding to the qp peak and the second a "tail" primarily composed of strength at energies above $\varepsilon_\Lambda^{qp}$. Specializing to the case of $k=0$ for simplicity, Eq. (76) becomes

$$z(0)\varepsilon_\Lambda^{qp}(0) + I_{tail}(0) = \Sigma_V^\Lambda(0), \tag{79}$$

where

$$\int d\omega\ \omega S_{tail}^\Lambda(k;\omega) \equiv I_{tail}(k), \tag{80}$$

and

$$\int d\omega\ \omega S_{qp}^\Lambda(k;\omega) = z(k)\varepsilon_\Lambda^{qp}(k). \tag{81}$$

Furthermore

$$S_{qp}^\Lambda(k;\omega) = z(k)\,\delta(\omega - \varepsilon_\Lambda^{qp}(k)) \tag{82}$$

has been used to obtain the contribution from the qp peak explicitly. The qp energy may be divided into two parts as in Eq. (68),

$$\varepsilon_\Lambda^{qp}(0) = \Sigma_V^\Lambda(0) + \Sigma_{2p1h}^\Lambda(0). \tag{83}$$

Now Eq. (79) may be rewritten as

$$z(0)\Sigma_V^\Lambda(0) + [z(0)\Sigma_{2p1h}^\Lambda(0) + I_{tail}(0)] = \Sigma_V^\Lambda(0). \tag{84}$$

For the $\Lambda$, $z(0)=0.87$, which is close enough to unity that Eq. (84) implies

$$z(0)\Sigma_{2p1h}^\Lambda(0) \approx -I_{tail}(0). \tag{85}$$

This may be interpreted to mean that the coupling to $2p$-$1h$ states at high energy shifts the qp peak from its HF value to lower energy. It may further be observed that for a strongly repulsive potential, $\Sigma_V^\Lambda(0)$ will be large and positive, as pointed out in Ref. [58]. For the NSC89 potential used in this work, the value is approximately 50 MeV. If the $\Lambda$ is to be bound at the experimentally observed level of approximately 30 MeV, then the larger $\Sigma_V^\Lambda(0)$ is, the larger $\Sigma_{2p1h}^\Lambda(0)$ must be to compensate. This in turn requires a larger value of $I_{tail}(0)$ to satisfy the sum rule. This constitutes an indirect association between the strength of the repulsive bare interaction and the required distribution of strength at high energy.

## IV. CONCLUSIONS

The spectral function for a $\Lambda$ hyperon in nuclear matter is calculated for the first time in this work. The structure of the spectral function is very similar to what is found for a nucleon. The chief qualitative difference lies in the coupled channel element which gives rise to threshold effects in the $\Lambda$ self-energy and spectral function. This behavior can be understood more fully by forging an analytic connection to established results for coupled channels in scattering theory. Consistent with the weaker binding of the $\Lambda$ to the medium as compared to nucleons, we also obtain a more quasiparticle-like spectral distribution of the sp strength. Nevertheless, a substantial reduction of 13% for the addition probability for adding a zero-momentum $\Lambda$ is obtained as compared to the free case. As for nucleons, a substantial portion of this removed strength is associated with the action of the tensor force, mediated by pions. In the present case, this effect occurs through the coupling to the intermediate $\Sigma N$ states in the effective interaction. The remaining portion of the removed strength is associated with the action of SRC which generate a momentum-independent high-energy tail in the spectral functions. The details of these spectral distribution of a $\Lambda$ can have modest consequences for the analysis of hypernuclear production probabilities and the mesonic decay width in a nuclear medium. The mesonic width, while Pauli suppressed in a nuclear environment despite strong correlations, may well show sensitivity to details of the lambda strength distribution. Finally, this work prepares the way for an examination of the weak decay properties of the $\Lambda$ in a nuclear environment with the influences of short-range correlations considered in consistent detail.

## ACKNOWLEDGMENT

This work is supported by the U.S. National Science Foundation under Grant Nos. PHY-9900713 and PHY-0140316.

[1] A. Gal, Adv. Nucl. Phys. **8**, 1 (1977).
[2] B. Povh, Annu. Rev. Nucl. Part. Sci. **28**, 1 (1978).
[3] R. E. Chrien and C. B. Dover, Annu. Rev. Nucl. Part. Sci. **39**, 113 (1989).
[4] B. F. Gibson and E. V. Hungerford III, Phys. Rep. **257**, 349 (1995).
[5] T. Miyoshi *et al.*, Phys. Rev. Lett. **90**, 232502 (2003).
[6] C. B. Dover and A. Gal, Prog. Part. Nucl. Phys. **12**, 171 (1983).
[7] T. Motoba, M. Bando, R. Wünsch, and J. Žofka, Phys. Rev. C **38**, 1322 (1988).
[8] A. A. Usmani, S. C. Pieper, and Q. N. Usmani, Phys. Rev. C **51**, 2347 (1995).
[9] D. Halderson, Phys. Rev. C **61**, 034001 (2000).

[10] M. Hjorth-Jensen, A. Polls, A. Ramos, and H. Müther, Nucl. Phys. **A605**, 458 (1996).
[11] I. Vidaña, A. Polls, A. Ramos, and M. Hjorth-Jensen, Nucl. Phys. **A644**, 201 (1998).
[12] J. Rożynek and J. Dabrowski, Phys. Rev. C **20**, 1612 (1979).
[13] Y. Yamamoto and H. Bandō, Prog. Theor. Phys. **73**, 189 (1983).
[14] Y. Yamamoto and H. Bandō, Prog. Theor. Phys. **83**, 254 (1990).
[15] A. Reuber, K. Holinde, and J. Speth, Nucl. Phys. **A570**, 543 (1994).
[16] H.-J. Schulze, A. Lejeune, J. Cugnon, M. Baldo, and U. Lombardo, Phys. Lett. B **355**, 21 (1995).
[17] H.-J. Schulze, M. Baldo, U. Lombardo, J. Cugnon, and A. Lejeune, Phys. Rev. C **57**, 704 (1998).
[18] J. Dabrowski and J. Rożynek, Prog. Theor. Phys. **105**, 923 (2001).
[19] M. Baldo, G. F. Burgio, and H.-J. Schulze, Phys. Rev. C **58**, 3688 (1998).
[20] V. G. J. Stoks and T.-S. H. Lee, Phys. Rev. C **60**, 024006 (1999).
[21] I. Vidaña, A. Polls, A. Ramos, M. Hjorth-Jensen, and V. G. J. Stoks, Phys. Rev. C **61**, 025802 (2000).
[22] M. Baldo, G. F. Burgio, and H.-J. Schulze, Phys. Rev. C **61**, 055801 (2000).
[23] I. Vidaña, A. Polls, A. Ramos, L. Engvik, and M. Hjorth-Jensen, Phys. Rev. C **62**, 035801 (2000).
[24] I. Vidaña, A. Polls, A. Ramos, and H.-J. Schulze, Phys. Rev. C **64**, 044301 (2001).
[25] A. Gal and C. B. Dover, Nucl. Phys. **A585**, 1c (1995).
[26] J. Schaffner-Bielich and A. Gal, Phys. Rev. C **62**, 034311 (2000).
[27] I. Bombaci, Phys. Rev. C **55**, 1587 (1997).
[28] M. Prakash and J. M. Lattimer, Nucl. Phys. **A639**, 433c (1998).
[29] M. M. Nagels, T. A. Rijken, and J. J. de Swart, Phys. Rev. D **12**, 744 (1975).
[30] M. M. Nagels, T. A. Rijken, and J. J. de Swart, Phys. Rev. D **15**, 2547 (1977).
[31] M. M. Nagels, T. A. Rijken, and J. J. de Swart, Phys. Rev. D **20**, 1633 (1979).
[32] P. M. M. Maessen, T. A. Rijken, and J. J. de Swart, Phys. Rev. C **40**, 2226 (1989).
[33] B. Holzenkamp, K. Holinde, and J. Speth, Nucl. Phys. **A500**, 485 (1989).
[34] T. A. Rijken, V. G. J. Stoks, and Y. Yamamoto, Phys. Rev. C **59**, 21 (1999).
[35] A. Ramos, A. Polls, and W. H. Dickhoff, Nucl. Phys. **A503**, 1 (1989).
[36] O. Benhar, A. Fabrocini, and S. Fantoni, Nucl. Phys. **A505**, 267 (1989).
[37] B. E. Vonderfecht, W. H. Dickhoff, A. Polls, and A. Ramos, Phys. Rev. C **44**, R1265 (1991).
[38] O. Benhar, A. Fabrocini, and S. Fantoni, Nucl. Phys. **A550**, 221 (1992).
[39] B. E. Vonderfecht, W. H. Dickhoff, A. Polls, and A. Ramos, Nucl. Phys. **A555**, 1 (1993).
[40] M. Hjorth-Jensen, M. Borromeo, H. Müther, and A. Polls, Nucl. Phys. **A551**, 580 (1993).
[41] E. Oset, P. Fernández de Córdoba, L. L. Salcedo, and R. Brockmann, Phys. Rep. **188**, 79 (1990).
[42] J. Cohen, Prog. Part. Nucl. Phys. **25**, 139 (1990).
[43] E. Oset and A. Ramos, Prog. Part. Nucl. Phys. **41**, 191 (1998).
[44] W. M. Alberico and G. Garbarino, Phys. Rep. **369**, 1 (2002).
[45] N. J. Robertson and W. H. Dickhoff, Phys. Rev. C (2004).
[46] A. A. Abrikosov, L. P. Gorkov, and I. E. Dzyloshinski, *Methods of Quantum Field Theory in Statistical Physics* (Dover, New York, 1975).
[47] A. L. Fetter and J. D. Walecka, *Quantum Theory of Many-Particle Systems* (McGraw-Hill, San Francisco, 1971).
[48] Y. Dewulf, W. H. Dickhoff, D. Van Neck, E. R. Stoddard, and M. Waroquier, Phys. Rev. Lett. **90**, 152501 (2003).
[49] R. V. Reid, Ann. Phys. (N.Y.) **50**, 411 (1968).
[50] C. B. Dover, D. J. Millener, and A. Gal, Phys. Rep. **184**, 1 (1989).
[51] M. I. Haftel and F. Tabakin, Nucl. Phys. **A158**, 1 (1970).
[52] M. Schmidt, G. Röpke, and H. Schulz, Ann. Phys. (N.Y.) **202**, 57 (1990).
[53] W. H. Dickhoff, C. C. Gearhart, E. P. Roth, A. Polls, and A. Ramos, Phys. Rev. C **60**, 064319 (1999).
[54] Q. N. Usmani and A. R. Bodmer, Phys. Rev. C **60**, 055215 (1999).
[55] J. M. Luttinger, Phys. Rev. **121**, 942 (1961).
[56] K. Hagiwara *et al.*, Phys. Rev. D **66**, 010001 (2002).
[57] B. C. Pearce and B. F. Gibson, Phys. Rev. C **40**, 902 (1989).
[58] A. Polls, A. Ramos, J. Ventura, S. Amari, and W. H. Dickhoff, Phys. Rev. C **49**, 3050 (1994).